nature neuroscience

ARTICLES

The Rho-GTPase cdc42 regulates neural progenitor fate at the apical surface

Silvia Cappello[1], Alessio Attardo[2], Xunwei Wu[3], Takuji Iwasato[4], Shigeyoshi Itohara[4], Michaela Wilsch-Bräuninger[2], Hanna M Eilken[1], Michael A Rieger[1], Timm T Schroeder[1], Wieland B Huttner[2], Cord Brakebusch[3] & Magdalena Götz[1,5]

Stem cell persistence into adulthood requires self-renewal from early developmental stages. In the developing mouse brain, only apical progenitors located at the ventricle are self-renewing, whereas basal progenitors gradually deplete. However, nothing is known about the mechanisms regulating the fundamental difference between these progenitors. Here we show that the conditional deletion of the small Rho-GTPase cdc42 at different stages of neurogenesis in mouse telencephalon results in an immediate increase in basal mitoses. Whereas cdc42-deficient progenitors have normal cell cycle length, orientation of cell division and basement membrane contact, the apical location of the Par complex and adherens junctions are gradually lost, leading to an increasing failure of apically directed interkinetic nuclear migration. These cells then undergo mitoses at basal positions and acquire the fate of basal progenitors. Thus, cdc42 has a crucial role at the apical pole of progenitors, thereby regulating the position of mitoses and cell fate.

The mechanisms regulating neurogenesis have received increased attention ever since it was accepted that neurogenesis can also continue into adulthood in the mammalian brain. For this to occur, some neural progenitors have to divide asymmetrically, in order for neural progenitors to be maintained into adulthood. Progenitors located at the apical side of the neuroepithelium in the zone lining the ventricle, the ventricular zone (VZ), self-renew and generate a progenitor cell as well as a postmitotic neuron during embryonic neurogenesis, whereas progenitors located basally above the VZ, in the subventricular zone (SVZ)[1], generate two neurons in most cases[2–5]. However, it is not known how these differences in fate are regulated at the molecular level.

The apically located VZ progenitors have an apico-basal polarity with a specialized apical membrane domain that is separated by the adherens junctions from the basolateral domain and is in contact with the basement membrane[6]. In contrast, the basally located SVZ progenitors contact neither the ventricle nor the basement membrane. Nevertheless, basal progenitors can exhibit an intrinsic polarity, such as the unequal distribution of the epidermal growth factor receptor at later developmental stages[7]. Basal (SVZ) progenitors further differ from apical (VZ) progenitors by the basal position of their mitosis, which is due to an incomplete or absent downward (basal to apical) movement of the nucleus during the G2/M phase[2–4]. In contrast, apical VZ cells perform interkinetic nuclear migration (INM), with their nuclei migrating during the course of cell division from a basally located phase of DNA synthesis to an apically located M phase and cytokinesis[8]. Similar movements have also been observed for astrocyte-like neural stem cells lining the lateral ventricle in the brain[9] that also seem to divide asymmetrically[10,11]. Thus, both during development and in adulthood, progenitors with apical contact to the ventricle undergo INM and self-renew.

Besides this difference in INM, apical and basal progenitors in the embryonic cortex also differ in the expression of some transcription factors. For example, Pax6 is largely contained in apical, but not basal, progenitors, whereas the transcription factor Tbr2 shows the complementary expression pattern[12], similar to NeuroD1, Svet1, vGlut2 and Cux2 (ref. 13).

Given the importance of SVZ progenitors in the phylogeny of the cerebral cortex, where SVZ progenitors become more and more predominant[14,15], we aimed to identify molecules involved in the regulation of VZ versus SVZ progenitor fate. A key difference between VZ and SVZ progenitors is their apico-basal polarity: only VZ progenitors contain a specialized apical membrane domain containing Par3, aPKC and prominin-1 (ref. 16, and see ref. 6 for a review). The Par complex is well known as a key regulator of apical polarity, junction formation and asymmetric cell division, and is regulated by the small Rho-GTPase cdc42 (refs. 17–19). Moreover, this complex has also been involved in the regulation of nuclear migration[20,21], prompting the idea that cdc42 may simultaneously regulate apical polarity by the Par complex and INM. However, despite the crucial role of this small Rho-GTPase in various processes[22], its function has so far not been elucidated in the developing nervous system.

[1]GSF, National Research Center for Environment and Health, Institute for Stem Cell Research, Ingolstädter Landstraße 1, D–85764 Neuherberg, Munich, Germany. [2]Max Planck Institute of Molecular Cell Biology and Genetics, Pfotenhauerstrasse 108, D-01307 Dresden, Germany. [3]Institute of Molecular Pathology, Faculty of Health Sciences, University of Copenhagen, Frederik V's Vej 11, DK-2100, Copenhagen, Denmark. [4]Laboratory for Behavioral Genetics, RIKEN Brain Science Institute (BSI), 2-1 Hirosawa, Wako-shi, Saitama 351-0198, Japan. [5]Institute of Physiology, University of Munich, Schillerstrasse 46, 80336 Munich, Germany. Correspondence should be addressed to M.G. (magdalena.goetz@gsf.de).

Received 1 June; accepted 10 July; published online 6 August 2006; doi:10.1038/nn1744

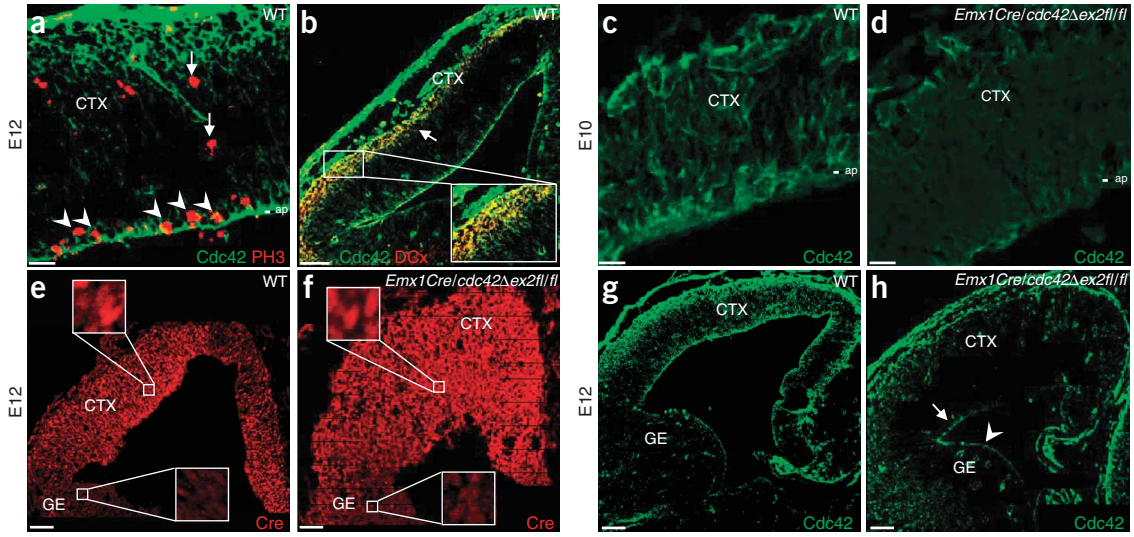

Figure 1 Cdc42 localization and deletion by Emx1::Cre in the cerebral cortex. (**a**–**h**) Micrographs of coronal sections of the cerebral cortex at E10 and E12, immunostained as indicated. Note that cdc42 immunoreactivity is concentrated in neurons (doublecortin-immunoreactive, inset in **b**) and at the apical side of progenitors (**a**,**b**; arrowheads, apical mitoses; arrows, basal mitoses (PH3-positive)). As early as E10, cdc42 immunoreactivity largely disappeared in the *Emx1*$^{Cre/cdc42\Delta ex2fl/fl}$ cortex compared to wild-type cortex (green in **c**,**d**). Panels **e** and **f** depict the Cre immunoreactivity (nuclear localization shown in insets in **e**,**f**) restricted to the cortex, causing the disappearance of cdc42 immunoreactivity (**g**,**h**) in most of the cortex except the lateral cortical regions (arrow in **h**) and the ganglionic eminence (arrowhead in **h**; no Cre expression in the ganglionic eminence: **e**,**f**) in the *Emx1*$^{Cre/cdc42\Delta ex2fl/fl}$ mice. The apical side of the neuroepithelium is indicated at the right side of the panels. CTX, cortex; DCx, doublecortin; GE, ganglionic eminence; ap, apical side. Scale bars: 20 μm in **a**; 10 μm in **c**,**d**; 50 μm in **b**,**e**–**h**.

RESULTS

Localization and deletion of cdc42 protein

First, we monitored Cdc42 localization throughout cortical neurogenesis (embryonic day, E, 10–16). Cdc42 immunoreactivity was enriched at the apical side of the VZ progenitors (**Fig. 1a–c**), consistent with its interaction with members of the apical Par complex. We also saw a high intensity of cdc42 immunostaining in the basally located postmitotic neurons, as detected by double staining with doublecortin (**Fig. 1b**). However, we were surprised to find little cdc42 immunoreactivity between these bands of high intensity, and most progenitors dividing at basal positions were hardly immunopositive (**Fig. 1a**).

To elucidate the function of cdc42 in cortical progenitors, we deleted exon2 of the *loxP*-flanked[23] *Cdc42* gene, by using a mouse line that expresses Cre in the Emx1 locus (Emx1::Cre, ref. 24) from around E9.5, just before the onset of neurogenesis in the developing cortex. In the cortex of *Emx1*$^{Cre/cdc42\Delta ex2fl/fl}$ mice, cdc42 immunoreactivity was already decreased at E10 (**Fig. 1c**,**d**; reduction of cdc42 immunoreactivity to 11% ± 1.5 of that in the wild type, four E10/11 embryos, two litters). As Cre expression showed a pronounced medial-to-lateral gradient similar to that of the endogenous Emx1 (**Fig. 1e**,**f**), cdc42 was still present in the lateral cortex, where Cre levels were too low to mediate recombination (arrow in **Fig. 1g**,**h**). Note the thickening of the cdc42-deficient cortex at E12 (**Fig. 1g**,**h**) that occurred at all rostro-caudal levels. Of *Emx1*$^{Cre/cdc42\Delta ex2fl/fl}$ mice, 75% survived to adulthood ($n = 36$; 9% of 25% expected); in these, only the lateral and piriform cortex still showed a normal layered organization (data not shown), whereas most of the mutant cortex was severely disorganized, was much thicker than the wild-type cortex and contained many hypertrophic glial fibrillary acidic protein (GFAP)-positive astrocytes (**Supplementary Fig. 1** online). Notably, the hippocampal region was also disorganized, but it was properly specified as visible by Math2 expression (**Supplementary Fig. 1**). To understand how this phenotype develops we examined the phenotype shortly after the onset of cdc42 deletion.

Increase in basal mitoses shortly after cdc42 deletion

At E10, the histological organization of the cdc42-deficient cortex was still normal. In light of the higher cdc42 immunoreactivity in apical versus basal progenitors, we examined whether the loss of cdc42 affected primarily the former but not the latter progenitor subtype. As VZ and SVZ progenitors divide at apical and basal positions, respectively, immunostaining for the phosphorylated form of histone H3 (PH3) present in late G2/M phase allows for discriminating between these distinct progenitors. In the wild-type cortex at E10, most PH3-positive cells in M phase were located apically, lining the ventricle; a few (3.3%) progenitors divided at some distance (5 cell diameters or more; see ref. 25) from the ventricle (**Fig. 2a**). However, upon cdc42 deletion, an increase in basal mitoses was readily detectable (**Fig. 2b**; sevenfold increase, to 20% of all mitoses). This phenotype became more severe during development, and at E12, about 70% of all progenitors divided at basal positions in the cdc42-deficient cortex, compared to 30% in the wild-type or heterozygous cortex (**Fig. 2c–i**). The high proportion of basal mitoses, as seen in the cdc42-deficient cortex, was never observed in the wild-type cortex, where apical mitoses are always predominant[2,25].

As basally dividing progenitors typically generate more (two) neurons per cell division than apically dividing progenitors (which only generate one[26,27]), we next examined the number of neurons after conditional deletion of cdc42. Despite the immediate increase in basally dividing cells at E10, neurogenesis was not affected: both the wild-type and cdc42-deficient cortices had the same proportion of neurons immunoreactive for βIII-tubulin, MAP2 (**Fig. 2a**,**b**,**f**) or HuC/D (data not shown). However, the number of neurons in cdc42-deficient cortex had increased by 30% 1 d later (**Fig. 2h**), and to twice the number of those in the wild-type cortex by E12 (**Fig. 2c**,**d**,**j**). Thus, the increase in neurogenesis in the cdc42-deficient cortex seemed to follow the increase in basal progenitors by 1 d, consistent with the observation that basal progenitors generate more neurons than those dividing apically[2–4].

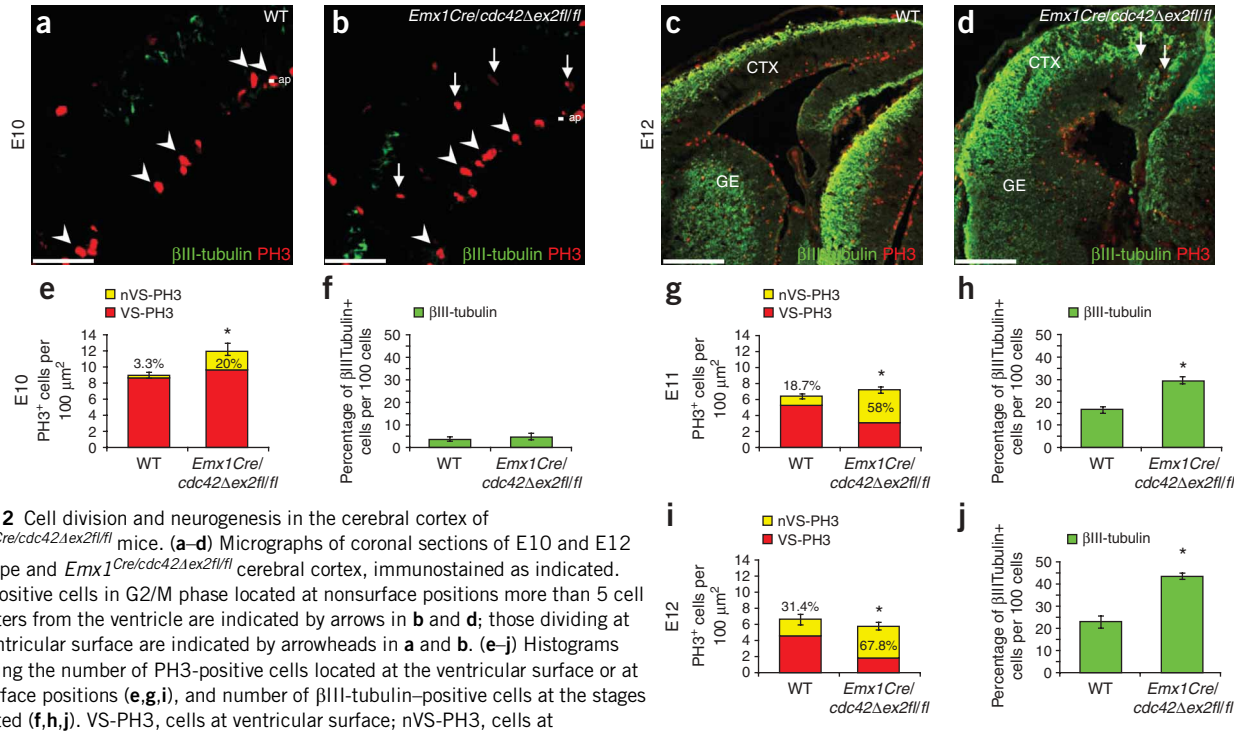

Figure 2 Cell division and neurogenesis in the cerebral cortex of *Emx1*$^{Cre/cdc42\Delta ex2fl/fl}$ mice. (**a**–**d**) Micrographs of coronal sections of E10 and E12 wild-type and *Emx1*$^{Cre/cdc42\Delta ex2fl/fl}$ cerebral cortex, immunostained as indicated. PH3-positive cells in G2/M phase located at nonsurface positions more than 5 cell diameters from the ventricle are indicated by arrows in **b** and **d**; those dividing at the ventricular surface are indicated by arrowheads in **a** and **b**. (**e**–**j**) Histograms depicting the number of PH3-positive cells located at the ventricular surface or at nonsurface positions (**e**,**g**,**i**), and number of βIII-tubulin–positive cells at the stages indicated (**f**,**h**,**j**). VS-PH3, cells at ventricular surface; nVS-PH3, cells at nonsurface positions. Note the significant increase in the proportion of PH3-positive cells at nonsurface positions and the number of neurons present in the cdc42-deficient cortex. Number of cells counted were as follows. **e**: wild-type $n = 2{,}275$; *Emx1*$^{Cre/cdc42\Delta ex2fl/fl}n = 2{,}368$; both 3 mice, 2 litters. **g**: wild-type $n = 654$; *Emx1*$^{Cre/cdc42\Delta ex2fl/fl}n = 701$; both 2 mice, 2 litters. **i**: wild-type $n = 1{,}043$; *Emx1*$^{Cre/cdc42\Delta ex2fl/fl}n = 1{,}036$; both 3 mice, 2 litters. **f**: wild-type $n = 1{,}141$; *Emx1*$^{Cre/cdc42\Delta ex2fl/fl}n = 1{,}334$; both 3 mice, 2 litters. **h**: wild-type $n = 1{,}359$; *Emx1*$^{Cre/cdc42\Delta ex2fl/fl}n = 1{,}334$; both 2 mice, 2 litters. **j**: wild-type $n = 4{,}168$; *Emx1*$^{Cre/cdc42\Delta ex2fl/fl}n = 2{,}400$; both 3 mice, 2 litters. Error bars represent s.e.m. Student's *t*-test, $^*P \leq 0.001$. Scale bars: 50 μm in **a**,**b**; 100 μm in **c**,**d**.

Normal orientation of cell division and cell cycle

Basal progenitors may arise as a result of alterations in the orientation of apically dividing progenitors[26,27], alteration in cell cycle phases that are different in basal progenitors[28], or defects in INM. As cdc42 has been implicated in centrosome positioning[29], regulation of cell cycle length[30] and nuclear movements[31], we examined to what extent these features are affected by the loss of cdc42.

Most progenitors in cortical neurogenesis divide vertically with respect to the ventricular surface (VS)[32–34], and this was also the case in the cdc42-deficient cortex when we quantified the orientation of mitoses in ana- and telophase at the ventricle at E10 and E12 (details in Methods; **Supplementary Fig. 2** online). Thus, deletion of cdc42 does not influence spindle orientation in the developing cerebral cortex.

Next, we examined cell cycle length by the cumulative labeling method described previously[35], using consecutive injections of the DNA-base analogon bromodeoxyuridine (BrdU). The number of BrdU-labeled cells among all cells (the labeling index) increased from 50% after a single injection (**Supplementary Fig. 2**; see also ref. 35) to almost 100% 5 h later, suggesting that 5 h are sufficient to label all the cycling cells (**Supplementary Fig. 2**). These data allowed us to calculate the cell cycle length (**Supplementary Fig. 2**), which was virtually identical in wild-type cortex (9.4 h) and cdc42-deficient cortex (9.6 h), in agreement with previous measurements[35]. However, only 20% of all progenitors were dividing basally at E10 in the cdc42-deficient cortex (**Fig. 2e**). We therefore measured the cell cycle length at E12, when most progenitors were already dividing basally in the mutant cortex (**Fig. 2i**). At this stage, in both wild-type and mutant cortex, the cell cycle length was increased and the labeling index decreased (to about 40%) after the first BrdU pulse (**Supplementary Fig. 2**, see also ref. 35). The percentage of BrdU-positive cells reached 100% after four consecutive BrdU injections, 9.5 h after the first BrdU injection when all cycling cells have been labeled by BrdU in S phase. We detected no significant differences in the cell cycle length between E12 wild-type and cdc42-deficient cortices, despite the strong phenotype in the position of cell division at this stage. Thus, the loss of cdc42 in corticogenesis does not affect cell cycle regulation.

However, we noted a different pattern in the distribution of BrdU-labeled cells in the mutant compared to wild-type cortex. In the caudal E12 cdc42-deficient cortex, many BrdU-positive cells were still located in a basal band after the first pulse of BrdU, similar to the distribution in the wild-type cortex (**Supplementary Fig. 3** online). Whereas cumulative BrdU labeling progressed only apically in the wild-type cortex, consistent with the apically directed nucleokinesis between the S and M phases (**Supplementary Fig. 3**), the cumulative BrdU labeling spread in both apical and further basal directions in the cdc42 mutant cortex (**Supplementary Fig. 3**). As these data suggest some aberrations in INM, we next examined the progression of cells in INM from the S to the M phase, by using a single BrdU pulse.

INM is affected *in vivo* but not *in vitro*

At E10, cells were labeled with BrdU in the S phase and their position was determined 30 min, 2 h and 4 h after BrdU injection. After 30 min, most BrdU-labeled nuclei were located in the basal part of the VZ, in both wild-type and cdc42-deficient cortices (**Fig. 3a**–**e**). Within 2 h, BrdU-labeled nuclei had moved apically in both wild-type and cdc42-deficient cortices, and no difference was as yet detectable between the genotypes (**Fig. 3e**). However, when the cortex was analyzed 4 h after BrdU injection, most of the wild-type BrdU-labeled nuclei had now reached the most apical positions, whereas some cdc42-deficient BrdU-labeled nuclei were apparently trailing behind and remained at basal

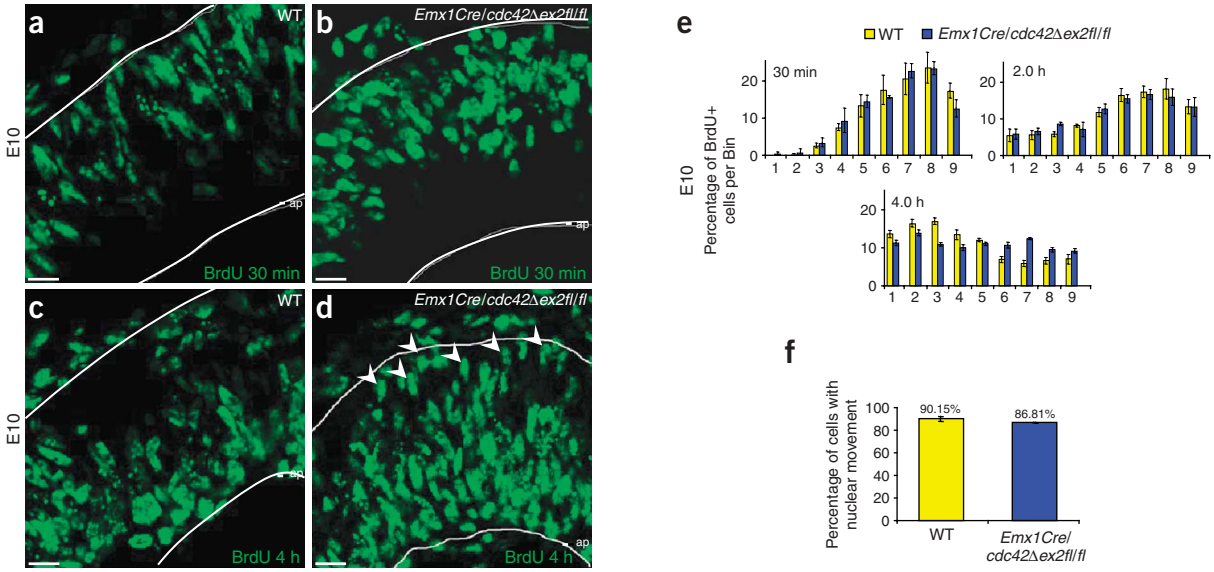

Figure 3 Analysis of interkinetic nuclear migration. (**a**–**d**) Fluorescent micrographs of coronal sections of E10 wild-type and $Emx1^{Cre/cdc42\Delta ex2fl/fl}$ cerebral cortex 30 min (**a**,**b**) or 4 h (**c**,**d**) after BrdU (green) injection. (**e**) Distribution of the BrdU-positive nuclei (wild-type: $n = 2{,}490$; $Emx1^{Cre/cdc42\Delta ex2fl/fl}$, $n = 1{,}879$; 6 mice, 5 litters) as percentage of all BrdU-positive nuclei per bin (one bin: 10-μm high and 100-μm wide; ref. 35). Note the increased number of BrdU-positive cells at basal positions (bins 6–9) 4 h after BrdU injection in the cdc42-deficient cortex (arrowheads in **d**). (**f**) Percentage of bipolar cells in dissociated cell cultures from E12 wild-type and $Emx1^{Cre/cdc42\Delta ex2fl/fl}$ cortices, showing bidirectional nuclear movement as analyzed by time-lapse video microscopy for 2 d (wild type: $n = 148$ cells, 4 mice, 2 litters; $Emx1^{Cre/cdc42\Delta ex2fl/fl}$: $n = 126$ cells, 3 mice, 2 litters). Error bars represent s.e.m. Scale bar, 10 μm.

positions (**Fig. 3c–e**). Notably, the increase in progenitors remaining at basal positions 4 h after the S phase (17%, **Fig. 3e**) closely resembled the increase in basal progenitors at this stage (20%, **Fig. 2e**). Thus, shortly after cdc42 deletion, some progenitors remain at a basal position between the S and M phases.

To clarify whether the defect in apically directed nuclear migration was a direct effect of cdc42 on nuclear movement, we cultured E12 wild-type and cdc42-deficient cortical cells and followed their nucleokineses by time-lapse videomicroscopy over 2 d (**Supplementary Videos 1** and **2** online). To examine nuclear movements in progenitors, we focused on long bipolar cells with progenitor morphology, as has been confirmed in sister cultures by nestin immunostaining. Notably, we detected no difference between wild-type and cdc42-deficient cells in terms of the proportion (90%, **Fig. 3f**) of bipolar cells making nuclear movements in both directions over a 48-h time period. Thus, in the absence of cdc42, nuclear movements can occur in dissociated cell

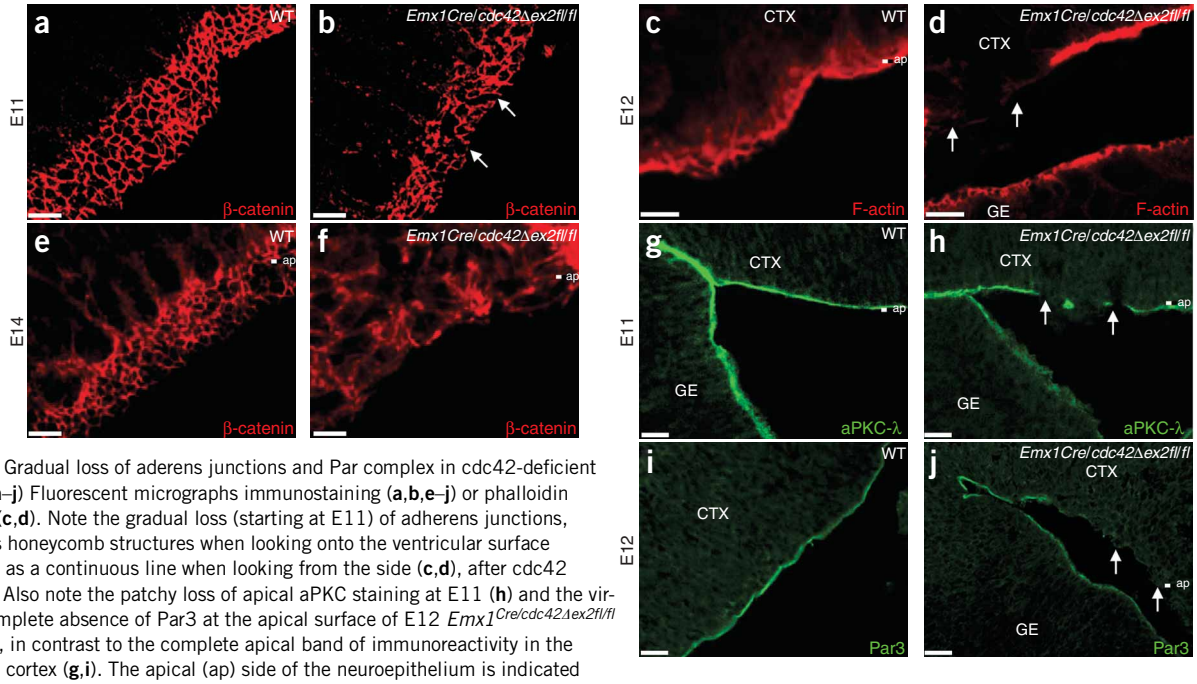

Figure 4 Gradual loss of aderens junctions and Par complex in cdc42-deficient cortex. (**a**–**j**) Fluorescent micrographs immunostaining (**a**,**b**,**e**–**j**) or phalloidin staining (**c**,**d**). Note the gradual loss (starting at E11) of adherens junctions, visible as honeycomb structures when looking onto the ventricular surface (**a**,**b**,**e**) or as a continuous line when looking from the side (**c**,**d**), after cdc42 deletion. Also note the patchy loss of apical aPKC staining at E11 (**h**) and the virtually complete absence of Par3 at the apical surface of E12 $Emx1^{Cre/cdc42\Delta ex2fl/fl}$ cortex (**j**), in contrast to the complete apical band of immunoreactivity in the wild-type cortex (**g**,**i**). The apical (ap) side of the neuroepithelium is indicated at the right side of panels **c**,**e**–**j**. Scale bars: 10 μm in **a**–**h**; 20 μm in **i**,**j**.

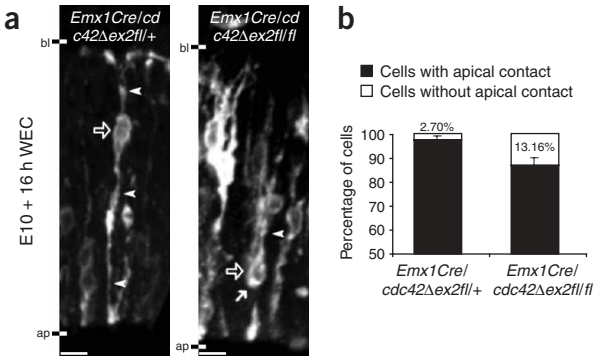

Figure 5 Retraction of the radial process from the apical surface. (**a**) GFP-labeled cells (white, electroporation at E10, culture for 16–20 h; arrows, cell bodies; arrowheads, processes) in coronal sections (60–130 μm) of the cerebral cortex. The apical (ap) and basal (bl) side of the neuroepithelium are indicated at the left side of the panels. (**b**) Percentage of cells with (black bars) and without (white bars) apical processes ($Emx1^{Cre/cdc42\Delta ex2fl/+}$: $n = 104$, 3 mice, 2 litters; $Emx1^{Cre/cdc42\Delta ex2fl/fl}$: $n = 92$, 2 mice, 2 litters). Error bars represent s.e.m. Scale bar, 10 μm.

cultures, suggesting that nucleokinesis itself is not directly affected by the loss of cdc42 protein.

Loss of apical Par complex and adherens junction

A key difference between dissociated progenitors and these cells *in vivo* is their organization; *in vivo*, progenitor cells are coupled by adherens junctions at the apical side and contact the basement membrane at the basal side. We therefore examined whether defects in anchoring at either side may explain the defects in nuclear movements *in vivo* but not *in vitro*.

First, we used laminin immunoreactivity to assess the anchoring of neuroepithelial cells labeled by RC2 to the basement membrane. RC2-positive processes contacted the basement membrane in the cdc42-deficient and wild-type cortices from E10 to E14 (**Supplementary Fig. 4** online and data not shown), suggesting that deletion of cdc42 does not lead to defects at the basal side of progenitors.

By immunostaining for adherens junction proteins such as β-catenin, cadherins or F-actin, we were able to visualize the characteristic honeycomb pattern of adherens junctions (viewed from the apical side) in both wild-type and cdc42 mutant cortices at E10 (**Supplementary Fig. 4**). By E11, however, we noted the first irregularities in this pattern in the cdc42-deficient cortex compared to that in the wild type (**Fig. 4a**,**b**); by E12, this had progressed to entire apical patches devoid of adherens junctions (**Fig. 4c**,**d**). By E14, hardly any pan-cadherin or β-catenin immunoreactivity (indicative of adherens junctions) was detectable in the cdc42-deficient cortex (**Fig. 4e**,**f**). Thus, the loss of cdc42 leads to the gradual disappearance of adherens junctions.

As cdc42 also recruits the Par complex to the apical side and to adherens junctions[16,17,36], we examined the atypical protein kinases C (aPKC-ι and aPKC-λ), Par3 and prominin-1, which is specifically localized in the apical membrane[37], upon deletion of cdc42 in the cortex. At E11, large patches were devoid of aPKC, Par3 or prominin-1 immunoreactivity in the cdc42 mutant cortex; by E12, this included most of the apical surface. In contrast, a continuous apical band was visible in wild-type cortex (**Fig. 4g–j** and data not shown). Thus, the loss of aPKC and Par3 immunoreactivity seems to precede the loss of adherens junctions upon cdc42 deletion, consistent with the role of this complex in the formation and maintenance of adherens junctions[38].

The increase in basal mitoses was detectable as early as E10, while no major defects in Par3 and/or aPKC immunoreactivity or in adherens junctions were as yet detectable. However, defects in 20% of apical endfeet may be difficult to resolve. We therefore conducted an *in vivo* electroporation of the cortices, in which we used a plasmid expressing

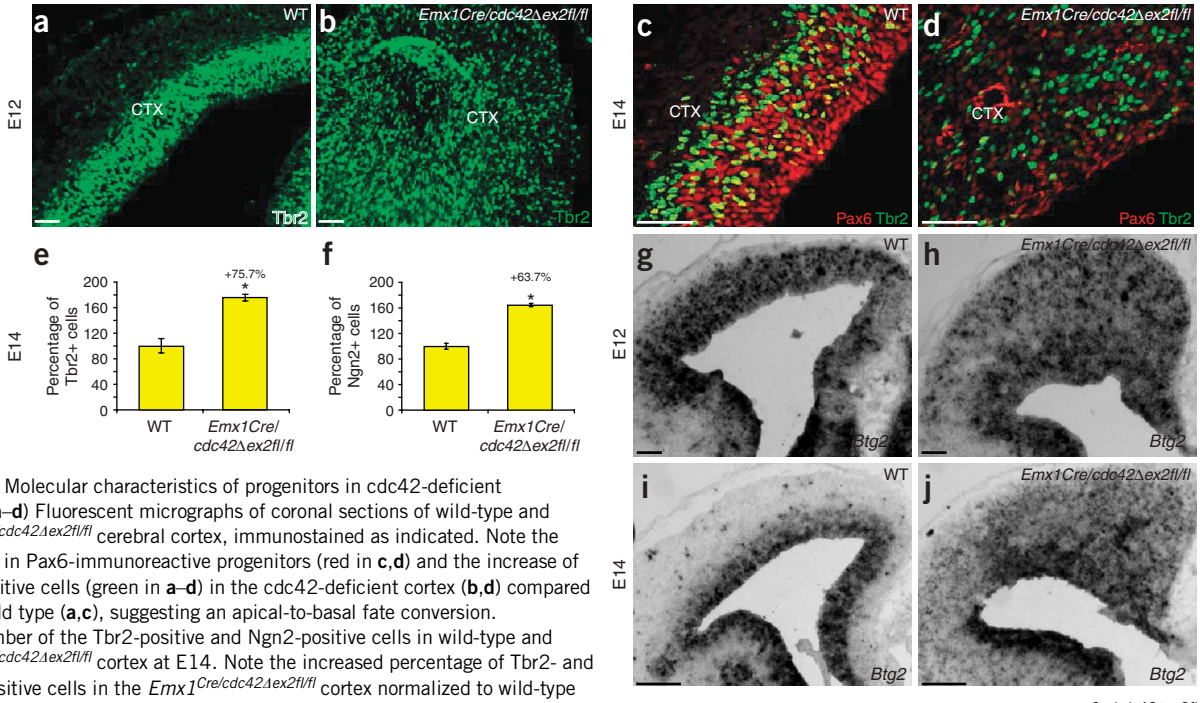

Figure 6 Molecular characteristics of progenitors in cdc42-deficient cortex. (**a**–**d**) Fluorescent micrographs of coronal sections of wild-type and $Emx1^{Cre/cdc42\Delta ex2fl/fl}$ cerebral cortex, immunostained as indicated. Note the decrease in Pax6-immunoreactive progenitors (red in **c**,**d**) and the increase of Tbr2-positive cells (green in **a**–**d**) in the cdc42-deficient cortex (**b**,**d**) compared to the wild type (**a**,**c**), suggesting an apical-to-basal fate conversion. (**e**,**f**) Number of the Tbr2-positive and Ngn2-positive cells in wild-type and $Emx1^{Cre/cdc42\Delta ex2fl/fl}$ cortex at E14. Note the increased percentage of Tbr2- and Ngn2-positive cells in the $Emx1^{Cre/cdc42\Delta ex2fl/fl}$ cortex normalized to wild-type cortex. Error bars represent s.e.m. Student's *t*-test, $^*P \leq 0.001$. Number of cells counted were as follows. **e**: wild-type $n = 1{,}684$; $Emx1^{Cre/cdc42\Delta ex2fl/fl}$ $n = 1{,}661$; both 2 mice, 2 litters). **f**: wild-type $n = 1{,}201$; $Emx1^{Cre/cdc42\Delta ex2fl/fl}$ $n = 3{,}368$; both 2 mice, 2 litters). (**g**–**j**) Expansion *of Btg2* mRNA in coronal sections of $Emx1^{Cre/cdc42\Delta ex2fl/fl}$ cerebral cortex (**h**,**j**) compared to the wild type (**g**,**i**). Scale bars: 50 μm in **a**–**d**,**g**,**h**; 100 μm in **i**,**j**.

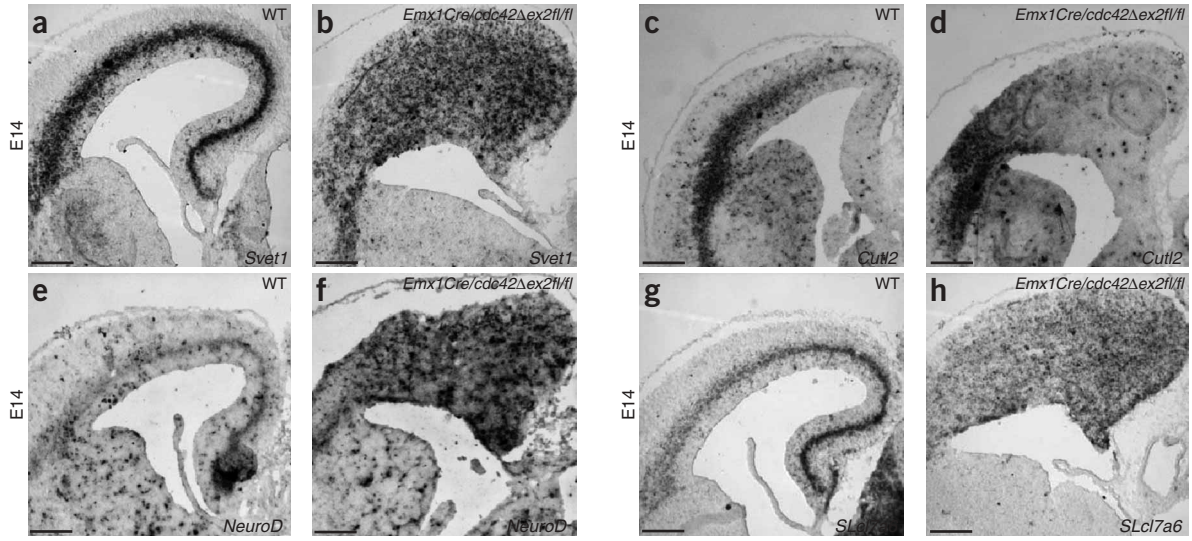

Figure 7 Molecular markers for basal progenitors (SVZ) expand in the cdc42-deficient cortex. (**a**–**h**) *In situ* hybridization of coronal sections of the E14 wild-type or *Emx1*$^{Cre/cdc42\Delta ex2fl/fl}$ cerebral cortex for the mRNA indicated in the panels. Note the spread of mRNA specific for SVZ progenitors in E14 *Emx1*$^{Cre/cdc42\Delta ex2fl/fl}$ cortex (**b**,**d**,**f**,**h**) compared to wild-type littermates (**a**,**c**,**e**,**g**). Scale bars, 100 μm.

green fluorescent protein (GFP) with the membrane localization sequence of GAP43 (GAP43-GFP), to label small groups of cortical progenitors. As the plasmid is taken up from the ventricle, this labels only those cells that have an apical process. We then cultured the electroporated embryos for 16–20 h (ref. 39) and, using multiphoton microscopy, looked for the presence or absence of an apical process (arrows in **Fig. 5a**) by conducting a three-dimensional (3D) reconstruction of single GFP-labeled cells in 60- to 130-μm-thick slices. Whereas only 2.7% of GFP-labeled cells lacked an apical process in the wild-type cortex, this percentage was increased to 13% in the cdc42-deficient cortex (**Fig. 5b**). Thus, a higher proportion of cells lose their apical contact as early as E10 in the cdc42-deficient cortex, consistent with their transformation into basal progenitors.

Molecular identity of basally dividing progenitors

The results presented above raise the possibility that the loss of cdc42 causes defects in apical process maintenance and INM, thereby leading to an increased number of progenitors dividing at basal rather than apical positions. These progenitors may still maintain the identity and fate of VZ progenitor cells, or they may convert to an SVZ fate. In the cdc42-deficient cortex, we noted a strong increase in cells immunoreactive for the transcription factor Tbr2, a marker of SVZ progenitors[12] (**Fig. 6a–d**). In contrast, Pax6 immunoreactivity, characteristic of VZ progenitors in the cortex[40], was strongly reduced (**Fig. 6c**,**d**). As SVZ progenitors are also heterogeneous—most generate two postmitotic neurons immediately, and a few continue to proliferate[5]—we examined *Btg2* (also known as *Tis21*) mRNA, which is upregulated in neurogenic progenitors before the generation of postmitotic neurons[2,33]. Indeed, *Btg2* was expressed all over the cdc42-deficient cortex (**Fig. 6e–h**), consistent with the neurogenic fate of the scattered basal progenitors in the cdc42-deficient cortex. Analysis of further SVZ markers such as *Neurog2*, the noncoding RNA *Svet1* (ref. 41), the bHLH gene *NeuroD1* (ref. 42), *Slc17a6* (also known as *vGluT2*; ref. 42) and *Cutl2* (also known as *Cux2*; ref. 13) revealed widespread localization of neurogenic SVZ cells in the E14 *Emx1*$^{Cre/cdc42\Delta ex2fl/fl}$ cortex, whereas expression of these genes was restricted to a small band in the cortex of wild-type littermates (**Figs. 6f** and **7**). Notably, some of these were expressed at earlier stages in the progenitor lineage (such as *Neurog2*, Tbr2, *Svet1*), whereas others, such as *Slc17a6* and *Cutl2*, appeared later. The last two still had the latero-medial gradient (**Fig. 7c**,**d**,**g**,**h**), anticipating neocortical arealization in the cdc42-deficient cortex. Taken together, these results suggest that basally dividing progenitors in the cdc42-deficient cortex acquire the fate of SVZ progenitors that are poised toward the generation of neurons.

Notably, the same phenotype of an immediate increase in Tbr2-positive basal progenitors followed by an increase in neurogenesis was also observed after cdc42 deletion at midneurogenesis (E13) by hGFAP-Cre (**Fig. 8a–h**). However, as the cortical plate had been established before recombination, the additional Tbr2-positive basal progenitors did not spread into this layer (compare **Figs. 8f** and **6b**).

DISCUSSION

So far, most of our knowledge about the function of Rho-GTPases in vertebrate neural cells is based on dominant-negative or constitutively active constructs used *in vitro*[22,43]. Besides concerns about the specificity of these constructs (for example, some effects observed with dominant-negative constructs could not be confirmed upon conditional deletion of cdc42; ref. 44), cdc42 function has, until now, not been examined in neural development *in vivo*. In this study, by conditionally deleting cdc42 at different developmental stages in cortical development, we showed that it has a key role in the maintenance of apico-basal polarity and self-renewing VZ progenitors. In contrast, cdc42 deletion had no effect on spindle orientation, cell cycle regulation or nuclear migration in dissociated cells. Thus, the main function of cdc42 in mammalian neurogenesis is to activate the Par complex to maintain adherens junction coupling and VZ progenitor fate. The loss of cdc42 resulted in the gradual conversion of apical VZ progenitors to basal SVZ progenitors that not only divided at basal positions, but also acquired the characteristic fate determinants of SVZ progenitors, such as *Neurog2*, Tbr2 and *NeuroD1*, as well as a higher rate of neuron generation. These data therefore demonstrate that cdc42 is crucial for the maintenance of VZ progenitors *in vivo*, and provide a first insight into the molecular mechanisms regulating the apical-to-basal transition of progenitors.

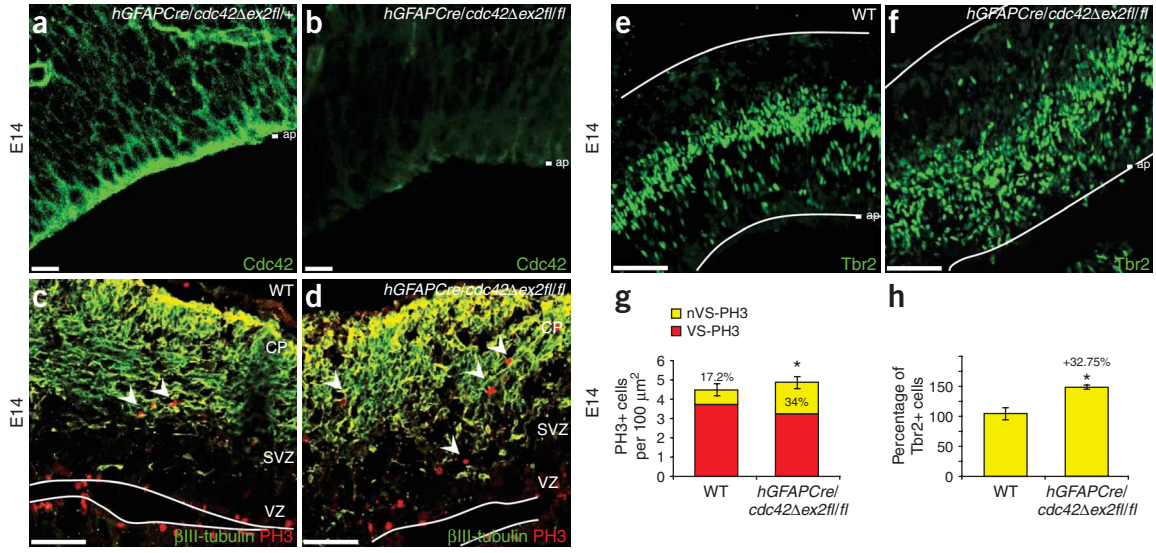

Figure 8 Cell division and neurogenesis in the cerebral cortex after removal of cdc42 by hGFAP-Cre. (**a**–**f**) Fluorescent micrographs of coronal sections of E14 wild-type and *hGFAP*$^{Cre/cdc42\Delta ex2fl/+}$ or *hGFAP*$^{Cre/cdc42\Delta ex2fl/fl}$ cerebral cortex, immunostained as indicated. Note the absence of cdc42 immunoreactivity in the E14 *hGFAP*$^{Cre/cdc42\Delta ex2fl/fl}$ cortex (**b**), compared to that in the *hGFAP*$^{Cre/cdc42\Delta ex2fl/+}$ cortex (**a**). Also note the increase in PH3-positive cells at nonsurface position in the *hGFAP*$^{Cre/cdc42\Delta ex2fl/fl}$ cortex (arrowheads in **d**) compared to wild-type cortex (arrowheads in **c**). (**g**) Histogram depicting the number of PH3-positive cells at surface and nonsurface positions (wild-type $n = 889$; *hGFAP*$^{Cre/cdc42\Delta ex2fl/fl}$ $n = 950$; both 2 mice, 2 litters). Concomitant to the increase in basal progenitors, the number of Tbr2-immunoreactive cells was increased (**e**,**f**,**h**; wild-type $n = 1{,}684$; *hGFAP*$^{Cre/cdc42\Delta ex2fl/fl}$ $n = 1{,}661$; both 2 mice, 2 litters). The apical (ap) side of the neuroepithelium is indicated at the right side of panels **a**,**b**,**e**,**f**. CTX, cortex; GE, ganglionic eminence; CP, cortical plate; SVZ, subventricular zone; VZ, ventricular zone. Error bars represent s.e.m. Student's *t*-test, $^*P \leq 0.001$. Scale bars: 10 μm in **a**,**b**; 50 μm in **c**–**f**.

Cdc42 function at the apical side of VZ progenitors

SVZ progenitors originate from VZ progenitors when the latter lose their contact with the apical surface[2–4]. Consistent with the enrichment of cdc42 immunoreactivity at the apical membrane, progenitors gradually lost their apical contacts in the cdc42-deficient cortex. This role of cdc42 in forming cellular junctions by activating the Par complex is well known in other epithelial cells[38]. Upon the formation of primordial adhesions by classical cadherins, the activation of the Par complex by cdc42 or Rac1 is required for the formation of tight junctions in epithelial cells. Taken together, these data imply that the apically concentrated cdc42 has a crucial function in the apical Par complex at the adherens junction, thereby distinguishing VZ from SVZ progenitors.

Our data further show that the role of cdc42 in the formation of junctions cannot be compensated for by Rac1 in neuroepithelial cells, in contrast to the observations in epidermal keratinocytes[45]. Moreover, whereas the loss of cdc42 in the hair follicle keratinocytes affects primarily canonical Wnt signaling[23], this is the case only at delayed stages in neuroepithelial cells (data not shown). These results underline the importance of studying the role of cdc42 in diverse cell types, as this versatile small GTPase exerts rather distinct functions in different cellular contexts. As we show here by time-lapse video microscopy, nuclear migration occurred normally in cdc42-deficient progenitors *in vitro*, whereas nuclear movements in postmitotic neurons are affected by manipulation of cdc42 function[46]. *In vivo*, however, nuclear migration of cortical progenitors was impaired after deletion of cdc42, suggesting that the loss of adherens junctions *in vivo* may be responsible for the impairment in the apically directed nuclear movements of neural progenitors. BrdU analysis revealed that the S phase still takes place at normal positions at early stages after cdc42 deletion, consistent with a normal basal cell migration during the G1 phase. In contrast, the apically directed INM was affected by the loss of cdc42, consistent with the need of an apical contact to exert a pulling force during apically directed movements between the S and M phases. *In vitro*, where anchoring is provided by the culture substrate, nuclei of cdc42-deficient neuroepithelial cells could migrate in both directions. Taken together, there is no direct effect of cdc42 on nucleokinesis in progenitor cells, but cdc42 is required at the apical side to maintain apico-basal polarity and junctional coupling.

The role of cdc42 in neural progenitor cell fate

The consequences of interference with junctional coupling in neural development have so far been associated with defects in signaling pathways, such as the canonical Wnt signaling[47] or Notch signaling[48,49]. Here we found that the deletion of cdc42 and adherens junction in the presence of normal Wnt and Notch signaling (data not shown) results in immediate fate conversion of VZ into SVZ progenitors. Cdc42-deficient progenitors not only lost Pax6 expression, but also upregulated Ngn2, Tbr2, NeuroD1, Svet1, VGlut2 and other molecules that are characteristic of neurogenic SVZ progenitors. These data therefore implicate, for the first time, signaling by the Rho-GTPase cdc42 in the maintenance of specific, self-renewing neural progenitor fate.

These results imply that either the location of mitosis, apico-basal polarity or activity of the Par complex is crucial for the maintenance of self-renewing VZ progenitors. In this regard, the difference in phenotype upon conditional deletion of aPKC-λ is very informative: in this mutant, despite the loss of adherens junction coupling and an increase in basal mitoses, neither SVZ markers such as Ngn2 (ref. 3) nor neurogenesis were increased[50]. This is notably different from the phenotype observed after cdc42 deletion at E10 by Emx1::Cre or at E13 (comparable to that in ref. 49) by hGFAP-Cre. The comparison of the phenotypes of these mutants thus suggests that the location of mitosis and the loss of apico-basal polarity may not be the only features determining VZ to SVZ fate transition, as these are also affected in the

aPKC-λ–deficient cortex. However, signaling via the Par complex should be different in the cdc42-deficient and aPKC-λ–deficient cortices, as the Par complex may still activate the aPKC-ζ in the aPKC-λ mutant cortex[50], but no activation of any aPKCs will occur in the absence of cdc42. These considerations suggest additional functions of the cdc42-activated Par complex, beyond regulating adherens junction coupling, that lead to the full conversion of apical into basal progenitors. Taken together, these data demonstrate a new role of cdc42 in neural progenitors, maintaining them in a self-renewing state, a prerequisite for the maintenance of stem cells into adulthood.

METHODS

Animals. Homozygous C57B1/6J//129/Sv-Cdc42fl/fl possessing *loxP* sites flanking exon 2 (ref. 23) were crossed to $Emx1^{Cre/cdc42\Delta ex2fl/+}$ or $hGFAP^{Cre/cdc42\Delta ex2fl/+}$ mice (day of plug = E0) to obtain the cdc42 mutants $Emx1^{Cre/cdc42\Delta ex2fl/fl}$ and $hGFAP^{Cre/cdc42\Delta ex2fl/fl}$. The same litter included phenotypic wild-type embryos with one or two *loxP*-flanked ('floxed') alleles and no Cre. Genotyping was performed by polymerase chain reaction (PCR), and each phenotypic analysis was done with at least 2–3 independent litters (see figure legends).

Immunohistochemistry. Brains of embryos were fixed in 4% paraformaldehyde (PFA) in phosphate-buffered saline (PBS) for 2–3 h at 4 °C, cryoprotected in 30% sucrose in PBS and cut, after embedding in Tissue-Tek, into12-μm-thick coronal sections at the cryostate. Sections were incubated in primary antibody overnight at 4 °C in 0.5% Triton X-100 and 10% normal goat serum in PBS. Primary antibodies were mouse antibody to aPKC-λ (Transduction Laboratories, 1:100), rat antibody to BrdU (ABCAM, 1:100; 30 min HCl 2M, 30 min borate buffer, pH 8.5), rabbit antibody to β-catenin (Sigma, 1:500), mouse antibody to cdc42 (IgG3, Santa Cruz, 1:100), rabbit antibody to Cre (Covance Research Products, 1:5,000), guinea pig antibody to doublecortin (Chemicon, 1:1,000), rat antibody to Ki67 (Dako Cytomation, 1:50), rabbit antibody to laminin (Chemicon, 1:40), mouse antibody to Ngn2 (IgG2a, gift from D.J. Anderson, California Institute of Technology, Pasadena, California, 1:10), mouse or rabbit antibody to pan-cadherin (Sigma, 1:200), rabbit antibody to PH3 (Biomol, 1:200), rabbit antibody to Par3 (gift from D. Lin, Mount Sinai Hospital, Toronto, 1:100), rat antibody to prominin1 (eBioscience, 1:100), mouse antibody to RC2 (IgM, gift from P. Leprince, University of Liège, Liège, Belgium, 1:500), rabbit antibody to Tbr2 (gift from R.F. Hevner, University of Washington, Seattle, Washington, 1:2,000, ref. 12) and mouse antibody to βIII-tubulin (IgG2b, Sigma, 1:100). F-actin filaments were visualized using rhodamine-labeled phalloidin (5 U ml^{-1}, Molecular Probes) by incubation for 30 min after previous blocking for 20 min in 0.1% Triton X-100 in PBS and for 1 h in 10% normal goat serum in PBS. Nuclei were visualized by incubating for 10 min with 0.1 μg ml^{-1} 4,6-diamidino-2-phenylindole (DAPI, Sigma) in PBS. Fluorescent secondary antibodies were used according to the manufacturer's protocol (Jackson ImmunoResearch or Southern Biotechnology) and sections were analyzed using Zeiss or Olympus laser-scanning microscopes.

BrdU labeling. BrdU was injected intraperitoneally into pregnant mice at E10 or E12 (50 mg per kg body weight). Cumulative BrdU labeling was performed by repeated intraperitoneal injections (3-h intervals) into pregnant mice. For the cell cycle analysis (**Supplementary Fig. 2**), the proportion of BrdU-positive nuclei among all DAPI-positive cells (which equals the labeling index, as almost all cells are dividing in E10 cortex) was determined at E10, and cell cycle parameters were calculated as described in ref. 35. For the cell cycle analysis at E12, the proportion of neurons was quantified by βIII-tubulin immunostaining and then subtracted from total number of DAPI-positive cells to calculate the labeling index. The INM was measured by quantifying the number of BrdU-positive cells in each bin, 30 min, 2 h and 4 h after a single BrdU injection (a bin was defined as a 10-μm-thick, 100-μm-long stripe parallel to the VS, with the apical-most bin as bin 1 and the basal-most bin as 9) (**Fig. 3e**).

***In situ* hybridization.** *In situ* plasmids were linearized, and digoxigenin-labeled RNA probes were made using DIG NTP labeling mix, RNA polymerases T3, T7 and Sp6, and RNase inhibitor (Roche) according to standard procedures. The RNA probes used were *Svet1* (ref. 41; gift from V. Tarabykin, Max-Planck Insitute for Experimental Medicine, Göttingen, Germany), *NeuroD1* (ref. 42), *Slc17a6* (also known as *vGluT2*; ref. 42), *Cutl2* (also known as *Cux2*; ref. 13; gift from C. Schuurmans, University of Calgary, Calgary, Canada) and *Btg2* (also known as *Tis21*).

Electron microscopy. E10 embryos were fixed in 1% glutaraldehyde in 0.1 M phosphate buffer. Then small pieces of the dorsal telencephalon were dissected and postfixed in aqueous 1% osmium tetroxide for 1 h at room temperature (18–30 °C). After dehydration and standard embedding in EMBed-812 (Science Services), 70-nm ultrathin sections were cut on a Leica UCT ultramicrotome (Leica Microsystems), poststained with uranyl acetate and lead citrate, and viewed in a Morgagni electron microscope (FEI). Images were taken with a MegaviewII camera (SIS).

Morphological analysis by GFP electroporation. E10 embryos were cultured in glass bottles with 1.5 ml medium as described previously[39]. After equilibration for 1 h, the telencephali were injected with 0.7 μg μl^{-1} of the GFP-containing construct (pCAGGs containing a GFP localized to the plasma membrane by the targeting sequence of the protein GAP43) in PBS, followed by a square pulse for transfection. After 16–20 h of further culture, embryos were decapitated and the heads were fixed in 4% PFA overnight, incubated in sucrose (30% in PBS), sliced (300–500 μm thick) with a tissue chopper (Vibratome 600 Mcllvain, Ted Pella), and embedded in agarose for imaging using an inverted Radiance 2100 multiphoton microscope (Bio-Rad) equipped with Nikon optics (ECLIPSE TE300) and a Mira 900 titanium:sapphire laser (Coherent) tuned to 900 nm, which was pumped by a Verdi 10 W solid-state laser (Coherent). Single Z stacks were collected (thickness of optical cube: 45–100 μm) in 0.5-μm steps, with 1024 × 1024 pixels and a scanning speed of 166–500 lines per s. Images were acquired using the Bio-Rad Laser Scan 2000 software. 3D reconstructions were computed using Imaris software (Imagic A.G.) in either the maximum intensity projection mode (MIP) or the blend-rendering mode; cells were scored manually for the presence or absence of apical contact. Neurons were identified by morphology (that is, position in the neuronal layer, nucleus orientation parallel to the apical surface, bi- or multipolar processes).

Dissociated cell culture and time-lapse video microscopy. Dissociated cortical cell cultures from E12 wild-type, $Emx1^{Cre/cdc42\Delta ex2fl/f+}$ and $Emx1^{Cre/cdc42\Delta ex2fl/fl}$ mice were prepared as described in ref. 32 and cultured at 37 °C, at a density of 8×10^5 cells per well, in neurobasal medium (Gibco) with 2% FCS, 5 ng ml^{-1} fibroblast growth factor (FGF2), B27 and 0.5 mM glutamine. After 12 h in 37 °C and 5% CO_2, the tissue culture plate was tightly sealed and time-lapse microscopy was performed with a cell observer (Zeiss) at a constant temperature of 37 °C (Pecon). Phase contrast pictures of at least two different positions per culture well were acquired at regular intervals of 10 min for 48 h with Axiovision Rel. 4.5 software (Zeiss) and an AxioCam HRm camera, according to the manufacturer's instructions. Images were assembled into a movie and analyzed frame by frame using Axiovision Rel. 4.5 and MetaMorph Offline (Version 6.1r4, Molecular Devices) software. Long bipolar cells with progenitor morphology were examined for bidirectional nuclear movement for 48 h (see **Supplementary Videos 1** and **2**).

Quantitative analysis. PH3-, Tbr2- and Ngn2-positive cells were quantified using Neurolucida software 6.0 (MicroBright Field). The cortex was defined as the area from the cortical hem to the pallial-subpallial boundary (confirmed by Pax6 immunostaining in mutants), and this area was measured. The number of PH3-positive cells within this area was quantified and calculated as the number of PH3-positive cells per 100 μm^2 (**Figs. 2e,g,i** and **8g**). Nonsurface positions were defined as those located more than 5 cell diameters from the VS (see ref. 25). Quantification of the number of neurons were performed on single optical sections by quantifying all βIII-tubulin–immunopositive cells and dividing by the number of DAPI-positive cells in a radial stripe comprising all cortical layers (**Fig. 2f,h,j**). Cells were scored as neurons only when βIII-tubulin immunostaining clearly surrounded a DAPI-positive nucleus.

The orientation of cell division was determined by measuring the angle of the cleavage plane of cells in ana- or telophase identified by propidium iodide staining. Angles between 0° and 30° were scored as horizontal division, angles

between 30° and 60° as oblique, and angles between 60° and 90° as vertical (see, for example, ref. 32.).

To quantify the amounts of cdc42 protein, the average of the signal intensity at the apical surface was measured at the confocal and set to 100% in the wild type, followed by measurements in a corresponding region of the cdc42-deficient cortex.

Quantifications are given as the mean ± s.e.m.; statistical significance was tested with the unpaired student's *t*-test ($P \leq 0.001$ indicated by an asterisk in the histograms).

Note: Supplementary information is available on the Nature Neuroscience website.

ACKNOWLEDGMENTS

We thank R.F. Hevner, D. Lin, D.J. Anderson, C. Schuurmans and V. Tarabykin for probes and antibodies; Y.-A. Barde for helpful comments on the manuscript; and M. Körbs, A. Bust, Z. Kirejczyk and B. DelGrande for excellent technical and secretarial assistance. M.G. is supported by the German Research Foundation. S.C. is recipient of a Marco Polo Fellowship.

AUTHOR CONTRIBUTIONS

S.C. did most of the experimental work. A.A. did the electroporation analysis. X.W. and C.B. generated the floxed cdc42 mice. T.I. and S.I. generated the Emx1::cre mice. M.W.-B. did the electronmicroscopic analysis. H.M.E., M.A.R. and T.T.S. taught and helped with the time-lapse analysis. W.B.H. was involved in writing the manuscript and designing experiments. M.G. designed the entire project, directed most of the experiments and wrote the manuscript together with S.C.

COMPETING INTERESTS STATEMENT

The authors declare that they have no competing financial interests.

Published online at http://www.nature.com/natureneuroscience
Reprints and permissions information is available online at http://npg.nature.com/reprintsandpermissions/

1. Smart, I.H. A pilot study of cell production by the ganglionic eminences of the developing mouse brain. *J. Anat.* **121**, 71–84 (1976).
2. Haubensak, W., Attardo, A., Denk, W. & Huttner, W.B. Neurons arise in the basal neuroepithelium of the early mammalian telencephalon: a major site of neurogenesis. *Proc. Natl. Acad. Sci. USA* **101**, 3196–3201 (2004).
3. Miyata, T. *et al.* Asymmetric production of surface-dividing and non-surface-dividing cortical progenitor cells. *Development* **131**, 3133–3145 (2004).
4. Noctor, S.C., Martinez-Cerdeno, V., Ivic, L. & Kriegstein, A.R. Cortical neurons arise in symmetric and asymmetric division zones and migrate through specific phases. *Nat. Neurosci.* **7**, 136–144 (2004).
5. Wu, S.X. *et al.* Pyramidal neurons of upper cortical layers generated by NEX-positive progenitor cells in the subventricular zone. *Proc. Natl. Acad. Sci. USA* **102**, 17172–17177 (2005).
6. Götz, M. & Huttner, W.B. The cell biology of neurogenesis. *Nat. Rev. Mol. Cell Biol.* **6**, 777–788 (2005).
7. Sun, Y., Goderie, S.K. & Temple, S. Asymmetric distribution of EGFR receptor during mitosis generates diverse CNS progenitor cells. *Neuron* **45**, 873–886 (2005).
8. Sauer, F.C. Mitosis in the neural tube. *J. Comp. Neurol.* **62**, 377–405 (1935).
9. Tramontin, A.D., Garcia-Verdugo, J.M., Lim, D.A. & Alvarez-Buylla, A. Postnatal development of radial glia and the ventricular zone (VZ): a continuum of the neural stem cell compartment. *Cereb. Cortex* **13**, 580–587 (2003).
10. Zhang, R. *et al.* Stroke transiently increases subventricular zone cell division from asymmetric to symmetric and increases neuronal differentiation in the adult rat. *J. Neurosci.* **24**, 5810–5815 (2004).
11. Alvarez-Buylla, A., Garcia-Verdugo, J.M. & Tramontin, A.D. A unified hypothesis on the lineage of neural stem cells. *Nat. Rev. Neurosci.* **2**, 287–293 (2001).
12. Englund, C. *et al.* Pax6, Tbr2, and Tbr1 are expressed sequentially by radial glia, intermediate progenitor cells, and postmitotic neurons in developing neocortex. *J. Neurosci.* **25**, 247–251 (2005).
13. Zimmer, C., Tiveron, M.C., Bodmer, R. & Cremer, H. Dynamics of Cux2 expression suggests that an early pool of SVZ precursors is fated to become upper cortical layer neurons. *Cereb. Cortex* **14**, 1408–1420 (2004).
14. Smart, I.H., Dehay, C., Giroud, P., Berland, M. & Kennedy, H. Unique morphological features of the proliferative zones and postmitotic compartments of the neural epithelium giving rise to striate and extrastriate cortex in the monkey. *Cereb. Cortex* **12**, 37–53 (2002).
15. Lukaszewicz, A. *et al.* G1 phase regulation, area-specific cell cycle control, and cytoarchitectonics in the primate cortex. *Neuron* **47**, 353–364 (2005).
16. Manabe, N. *et al.* Association of ASIP/mPAR-3 with adherens junctions of mouse neuroepithelial cells. *Dev. Dyn.* **225**, 61–69 (2002).
17. Hutterer, A., Betschinger, J., Petronczki, M. & Knoblich, J.A. Sequential roles of Cdc42, Par-6, aPKC, and Lgl in the establishment of epithelial polarity during *Drosophila* embryogenesis. *Dev. Cell* **6**, 845–854 (2004).
18. Etienne-Manneville, S., Manneville, J.B., Nicholls, S., Ferenczi, M.A. & Hall, A. Cdc42 and Par6-PKCzeta regulate the spatially localized association of Dlg1 and APC to control cell polarization. *J. Cell Biol.* **170**, 895–901 (2005).
19. Lin, D. *et al.* A mammalian PAR-3-PAR-6 complex implicated in Cdc42/Rac1 and aPKC signalling and cell polarity. *Nat. Cell Biol.* **2**, 540–547 (2000).
20. Schaar, B.T. & McConnell, S.K. Cytoskeletal coordination during neuronal migration. *Proc. Natl. Acad. Sci. USA* **102**, 13652–13657 (2005).
21. Tsai, L.H. & Gleeson, J.G. Nucleokinesis in neuronal migration. *Neuron* **46**, 383–388 (2005).
22. Govek, E.-E., Newey, S.E. & Van Aelst, L. The role of the Rho GTPases in neuronal development. *Genes Dev.* **19**, 1–49 (2005).
23. Wu, X. *et al.* Cdc42 controls progenitor cell differentiation and beta-catenin turnover in skin. *Genes Dev.* **20**, 571–585 (2006).
24. Iwasato, T. *et al.* Cortex-restricted disruption of NMDAR1 impairs neuronal patterns in the barrel cortex. *Nature* **406**, 726–731 (2000).
25. Haubst, N. *et al.* Molecular dissection of Pax6 function: the specific roles of the paired domain and homeodomain in brain development. *Development* **131**, 6131–6140 (2004).
26. Miyata, T., Kawaguchi, A., Okano, H. & Ogawa, M. Asymmetric inheritance of radial glial fibers by cortical neurons. *Neuron* **31**, 727–741 (2001).
27. Noctor, S.C., Flint, A.C., Weissman, T.A., Dammerman, R.S. & Kriegstein, A.R. Neurons derived from radial glial cells establish radial units in neocortex. *Nature* **409**, 714–720 (2001).
28. Calegari, F., Haubensak, W., Haffner, C. & Huttner, W.B. Selective lengthening of the cell cycle in the neurogenic subpopulation of neural progenitor cells during mouse brain development. *J. Neurosci.* **25**, 6533–6538 (2005).
29. Palazzo, A.F. *et al.* Cdc42, dynein, and dynactin regulate MTOC reorientation independent of Rho-regulated microtubule stabilization. *Curr. Biol.* **11**, 1536–1541 (2001).
30. Olson, M.F., Ashworth, A. & Hall, A. An essential role for Rho, Rac, and Cdc42 GTPases in cell cycle progression through G1. *Science* **269**, 1270–1272 (1995).
31. Gomes, E.R., Jani, S. & Gundersen, G.G. Nuclear movement regulated by Cdc42, MRCK, myosin, and actin flow establishes MTOC polarization in migrating cells. *Cell* **121**, 451–463 (2005).
32. Heins, N. *et al.* Emx2 promotes symmetric cell divisions and a multipotential fate in precursors from the cerebral cortex. *Mol. Cell. Neurosci.* **18**, 485–502 (2001).
33. Kosodo, Y. *et al.* Asymmetric distribution of the apical plasma membrane during neurogenic divisions of mammalian neuroepithelial cells. *EMBO J.* **23**, 2314–2324 (2004).
34. Chenn, A. & McConnell, S.K. Cleavage orientation and the asymmetric inheritance of Notch1 immunoreactivity in mammalian neurogenesis. *Cell* **82**, 631–641 (1995).
35. Takahashi, T., Nowakowski, R.S. & Caviness, V.S. The cell cycle of the pseudostratified ventricular epithelium of the embryonic murine cerebral wall. *J. Neurosci.* **15**, 6046–6057 (1995).
36. Joberty, G., Petersen, C., Gao, L. & Macara, I.G. The cell-polarity protein Par6 links Par3 and atypical protein kinase C to Cdc42. *Nat. Cell Biol.* **2**, 531–539 (2000).
37. Weigmann, A., Corbeil, D., Hellwig, A. & Huttner, W.B. Prominin, a novel microvilli-specific polytopic membrane protein of the apical surface of epithelial cells, is targeted to plasmalemmal protrusions of non-epithelial cells. *Proc. Natl. Acad. Sci. USA* **94**, 12425–12430 (1997).
38. Macara, I.G. Parsing the polarity code. *Nat. Rev. Mol. Cell Biol.* **5**, 220–231 (2004).
39. Eto, K. & Osumi-Yamashita, N. Whole embryo culture and the study of postimplantation mammalian development. *Dev. Growth Differ.* **37**, 123–132 (1995).
40. Gotz, M., Stoykova, A. & Gruss, P. Pax6 controls radial glia differentiation in the cerebral cortex. *Neuron* **21**, 1031–1044 (1998).
41. Tarabykin, V., Stoykova, A., Usman, N. & Gruss, P. Cortical upper layer neurons derive from the subventricular zone as indicated by Svet1 gene expression. *Development* **128**, 1983–1993 (2001).
42. Schuurmans, C. *et al.* Sequential phases of cortical specification involve Neurogenin-dependent and -independent pathways. *EMBO J.* **23**, 2892–2902 (2004).
43. Jaffe, A.B. & Hall, A. RHO GTPases: biochemistry and biology. *Annu. Rev. Cell Dev. Biol.* **21**, 247–269 (2005).
44. Czuchra, A. *et al.* Cdc42 is not essential for filopodium formation, directed migration, cell polarization, and mitosis in fibroblastoid cells. *Mol. Biol. Cell* **16**, 4473–4484 (2005).
45. Mertens, A.E., Rygiel, T.P., Olivo, C., van der Kammen, R. & Collard, J.G. The Rac activator Tiam1 controls tight junction biogenesis in keratinocytes through binding to and activation of the Par polarity complex. *J. Cell Biol.* **170**, 1029–1037 (2005).
46. Kholmanskikh, S.S. *et al.* Calcium-dependent interaction of Lis1 with IQGAP1 and Cdc42 promotes neuronal motility. *Nat. Neurosci.* **9**, 50–57 (2006).
47. Machon, O., van den Bout, C.J., Backman, M., Kemler, R. & Krauss, S. Role of [beta]-catenin in the developing cortical and hippocampal neuroepithelium. *Neuroscience* **122**, 129–143 (2003).
48. Hatakeyama, J. Hes genes regulate size, shape and histogenesis of the nervous system by control of the timing of neural stem cell differentiation. *Development* **131**, 5539–5550 (2004).
49. Li, H.S. *et al.* Inactivation of Numb and Numblike in embryonic dorsal forebrain impairs neurogenesis and disrupts cortical morphogenesis. *Neuron* **40**, 1105–1118 (2003).
50. Imai, F. *et al.* Inactivation of aPKClambda results in the loss of adherens junctions in neuroepithelial cells without affecting neurogenesis in mouse neocortex. *Development* **133**, 1735–1744 (2006).